Cerebral Cortex September 2012;22:2016–2023
doi:10.1093/cercor/bhr277
Advance Access publication October 8, 2011

Visualization of Cortical Lamination Patterns with Magnetic Resonance Imaging

Daniel Barazany and Yaniv Assaf

Department of Neurobiology, The George S. Wise Faculty of Life Sciences, Tel Aviv University, Tel Aviv 69978, Israel

Address correspondence to Dr Yaniv Assaf, Department of Neurobiology, The George S. Wise Faculty of Life Sciences, Tel Aviv University, Tel Aviv 69978, Israel. Email: asafyan@zahav.net.il.

The ability to image the cortex laminar arrangements in vivo is one of the holy grails of neuroscience. Recent studies have visualized the cortical layers ex vivo and in vivo (on a small region of interest) using high-resolution T_1/T_2 magnetic resonance imaging (MRI). In this study, we used inversion-recovery (IR) MRI to increase the sensitivity of MRI toward cortical architecture and achieving whole-brain characterization of the layers, in vivo, in 3D on humans and rats. Using the IR measurements, we computed 3D signal intensity plots along the cortex termed corticograms to characterize cortical substructures. We found that cluster analyses of the multi-IR images along the cortex divides it into at least 6 laminar compartments. To validate our observations, we compared the IR-MRI analysis with histology and revealed a correspondence, although these 2 measures do not represent similar quantities. The abilities of the method to segment the cortex into layers were demonstrated on the striate cortex (visualizing the stripe of Gennari) and on the frontal cortex. We conclude that the presented methodology can serve as means to study and characterize individual cortical architecture and organization.

Keywords: BAs, cortical layers, IR-MRI, microstructure, rat and human brain

Introduction

More than 100 years ago, Brodmann, Von-Economo, and others discovered the cellular cytoarchitecture of neuronal tissues (cortical cytoarchitecture) (von Economo and Koskinas 1925; Brodmann and Garey 1999). Six distinct layers of cell structures were identified, having similar composition and order throughout the cortex but differing in their fractional volumes between regions. This histological, cytoarchitectonic feature of the cortex is the basis of its parcellation into neuroanatomical regions (e.g., Brodmann's areas [BAs]). The cortical layers can be characterized not only by their cytoarchitecture but also by the myeloarchitecture (the density and content of myelin across the cortex) (Vogt 1911). Such staining was also the base of brain parcellation and provided similar neuroanatomical maps to the cytoarchitecture segmentation (Annese et al. 2004).

There is a growing interest to obtain an in vivo imaging modality that enables visualization of macroscopic cell structure arrangements for the whole brain and in 3D. Magnetic resonance imaging (MRI) is the noninvasive, in vivo imaging modality that provides the best spatial anatomical details of the human brain. Visualizing the cortical layers presents various challenges: 1) extremely high resolution is required to resolve the layers, leading to long acquisition times and the need for a high magnetic field to overcome low signal-to-noise levels; 2) MRI detects water and thus is not specific to cell morphology, in general and to neuronal cell architecture in particular; and 3) the MRI signal profile along the cortex at conventional methods and resolution seems to be isointense and therefore cannot be segmented into cortical substructures.

Despite these limitations, T_1 and T_2 MRI contrast mechanisms were suggested for discrimination between the layers. Already in 1992, Clark et al. (1992) showed that high-resolution (~400 μm^2) T_1-weighted MRI can be used to visualize the border between the striate (BA 17) and extrastriate cortex (BAs 18 and 19). The ability to discriminate between these regions was attributed to the heavily myelinated layer IV of area 17 (stria of Gennari). A discrimination of the stria of Gennari was obtained by T_2-weighted images as well (Barbier et al. 2002; Walters et al. 2003), indicating that high-resolution MRI is potentially sensitive to the cortical microstructural arrangement and architecture. Indeed, this observation was recently demonstrated on the mouse brain (Boretius et al. 2009).

Several works followed this approach and acquired high-resolution anatomical MR images of excised cortical tissue and small sections of in vivo human brains (Barbier et al. 2002; Fatterpekar et al. 2002; De Vita et al. 2003; Walters et al. 2003; Bridge et al. 2005; Clare and Bridge 2005; Eickhoff et al. 2005; Bridge and Clare 2006; Duyn et al. 2007). Variations of the MR signal profiles perpendicular to the cortex were suggested to be sensitive to the underlying microstructure and cyto/myeloarchitectonic arrangements (Barbier et al. 2002; Fatterpekar et al. 2002; Walters et al. 2003; Eickhoff et al. 2005; Duyn et al. 2007). Nevertheless, the contrast between the layers in most cortical regions as seen in the T_1- or T_2-weighted cortical profiles is not strong enough to allow a robust whole-brain segmentation of the cortical layers with MRI, leading to the conclusion that increased image contrast is needed. A few works did attempt to enhance the contrast between the layers by using contrast agents that are less applicable for routine human brain imaging (Angenstein et al. 2007; Silva et al. 2008).

In the present study, we utilized inversion-recovery (IR) MRI to acquire multi T_1-weighted images with increased contrast between cortical substructures (for additional background on the IR-MRI method, please refer to the Supplementary Material—additional background). As indicated above, it is well-accepted that myelination causes shortening of the T_1, and T_1 will therefore decrease from the outer to the inner layers of the cortex (Clark et al. 1992). We exploited the T_1 properties

of gray matter (as imaged with IR-MRI) to discriminate between laminar compartments within the cortex. To that end, we hypothesize that cortical substructures will have distinct T_1 properties that become visible and analyzable using the high contrast of IR-MRI. In the present work, we argue that by using a series of IR images, a laminar pattern of cortical substructures can be obtained for the whole brain, in 3D. We propose a framework to visualize (corticogram) and quantify (by cluster analysis) such information. We show that our approach can identify and quantify cortical substructures. We applied this approach to discriminate between the cortical laminar compartments in vivo in human and rat brains and validated the results with histology.

Materials and Methods

Subjects

Humans

Fifteen healthy subjects were recruited for this study, 8 males and 7 females, 25–35 years of age. Subjects were neurologically and radiologically healthy, with no history of neurological diseases, and normal appearance of clinical MRI protocol. The imaging protocol was approved by the institutional review board of the Tel Aviv Sourasky Medical Center, where the MRI investigations were performed. All subjects provided signed informed consent before enrollment in the study.

Rats

Two male, 7-month-old Wistar rats were used in this study. During the imaging protocol, the rats were anesthetized with approximately 2% isoflurane (in oxygen). Following the MRI, the rat brains were euthanized and prepared for histology (see below). The protocol was approved by the Tel Aviv University ethics committee on animal research.

Magnetic Resonance Imaging

Human Experiments

MRI was performed on a 3T General Electric (GE) scanner with an 8-channel radio frequency coil and a 50 mT/m gradient system. The protocol included conventional clinical screening sequences (sagittal spin-echo T_1, axial fast spin-echo [FSE] T_2, and axial fluid attenuated inversion recovery [FLAIR]) covering the whole brain and lasted 15 min. Then, a series of IR FSE images were acquired. Here, we utilized the inversion time (TI) parameter in IR to produce a series of different image contrasts. More in-depth description of the IR methodology is given in the Supplementary Material. The IR FSE sequence was acquired with the following parameters: time repetition (TR)/echo time (TE) = 11 000/14 ms with TI varied at the following values: 230, 432, 575, 760, 920, 1080, and 1380 ms. The TI of 230 ms was used to produce white matter (WM) nulled image. One whole left hemisphere acquisition was done in the sagittal plane with a matrix of 512 × 384 (reconstructed to 512 × 512) with a final pixel size of 0.430 × 0.430 mm^2 in various slice thickness (3 mm [n = 2], 2.5 mm [n = 2], 1.8 mm [n = 1], and 1.5 mm [n = 6]). Additional experiments with slice thickness of 1.5 mm (n = 4) were acquired at the axial plane to investigate and visualize the stria of Gennari at the striate cortex. The total acquisition time for the multi IR-MRI data lasted 45 min.

In addition to the screening and the multiple IR data set, conventional T_1 spoiled gradient recalled echo (SPGR) image (TR/TE/TI/flip angle = 9.3/3.8/450/13°) was acquired at 1 × 1 × 1 mm^3 resolution. The total MRI protocol lasted 60 min.

Rat Experiments

MRI was performed on a 7T/30 Bruker scanner with a 400 mT/m gradient system. The research protocol was similar to the human experiments with slight modifications, as given below. The TIs were varied for each experiment using the following values: 480, 820, 920, 990, 1040, 1140, 1250, and 2000 ms. Whole-brain acquisitions were acquired at the coronal plane with a matrix of 256 × 192 (reconstructed to 256 × 256) with a final pixel size of 125 × 125 μm^2 and slice thickness of 400 μm. Total acquisition time for the IR-MRI data set was around 1 h.

Image Analysis

T_1 Analysis

T_1 analysis was done on a pixel-by-pixel basis by fitting the entire IR data set to an exponential decay function, according to the following formula: $M(\mathrm{TI}_i)/M_0 = 1-2e^{(-\mathrm{TI}_i/T_1)}$, Where $M(\mathrm{TI}_i)$ is the magnetization at the ith TI and M_0 is the magnetization at TI = 0 ms. Following successful fitting, each pixel was assigned a single T_1 value. Although an optimal calculation of the T_1 will require a more lengthy experiment, we used this analysis to get an estimate of the relative T_1variations along the cortex.

Corticogram

Characterization of the IR properties along the cortex was achieved by a 3D plot of IR signals variation along the cortex (corticogram). In that plot, a rectangular region of interest (ROI) perpendicular to the cortex was defined; the y-axis of this ROI represents the cortical axis from the outer edge to its inner edge, whereas the x-axis represents the region borders. The signal was averaged along the x-axis and plotted in 3D versus the TI and the cortical axis (y-axis of the ROI). This procedure was replicated for different cortical regions and emphasizes the power of IR-MRI in characterizing the cortical architecture and distinguishing between different cortical regions.

Cluster Analysis

Visualization and quantification of the lamination structure from the multi-IR images was done according to a multispectral image analysis (Yovel and Assaf 2007). Briefly, following the coregistration (to correct for head movements), the cortex was automatically segmented based on the SPGR, FLAIR, and WM-zeroed IR images. Basic contrast enhancement was used on the segmented cortex to exclude outlier pixels, thereby stretching the dynamic range of the image. Cluster analysis based on the multiparametric data was then performed, including the following steps: 1) normalizing the data to create a uniform scale between the different imaging methods, 2) transforming the data into its principle component analysis space to increase the variance, and 3) running a clustering algorithm such as "k-means"; the number of k-cluster is set to 5 or 6 according to the results of the Gaussian mixture analysis (Fig. 1 and see Supplementary Fig. *S*1).

Comparison with Brodmann's Map

The results of the MRI methodology were validated by comparing the relative thickness or fractional volume of each of the IR clusters with histology data according to the standard Brodmann (Brodmann and Garey 1999) cytoarchitectonic segmentation as an histological reference. A template of Brodmann's map (MRIcron, Chris Roden) was registered and normalized to the high-resolution SPGR of each subject, so the cortical substructures' regional clusters could be assigned to different BAs. We report here this analysis on 10 BA of the frontal lobe, although a similar analysis can be applied to any set of regions. Statistical analysis was performed using a factorial 5 (IR layers) by 10 (BA regions) repeated-measure analysis of variance (ANOVA).

Histology

The rat brains were extracted and fixated with formalin 4%, washed with tap water, and dehydrated with a graded series of ethanol (70%, 96%, and 100%) and chloroform until they sank to the bottom of the test tube. The brains were then embedded in a paraffin solution (Merck, NJ) for a few days for hardening, after which the whole brain was cut serially in the coronal plane (2-μm section thickness) with a sliding microtome (Leica Microsystems SM2500, Nussloch, Germany). The sections were mounted on gelatin slides and postfixated with a solution of sodium phosphoric acid and formalin 37% over 2 days. A deparaffinization phase was executed by Xylol and a downgraded

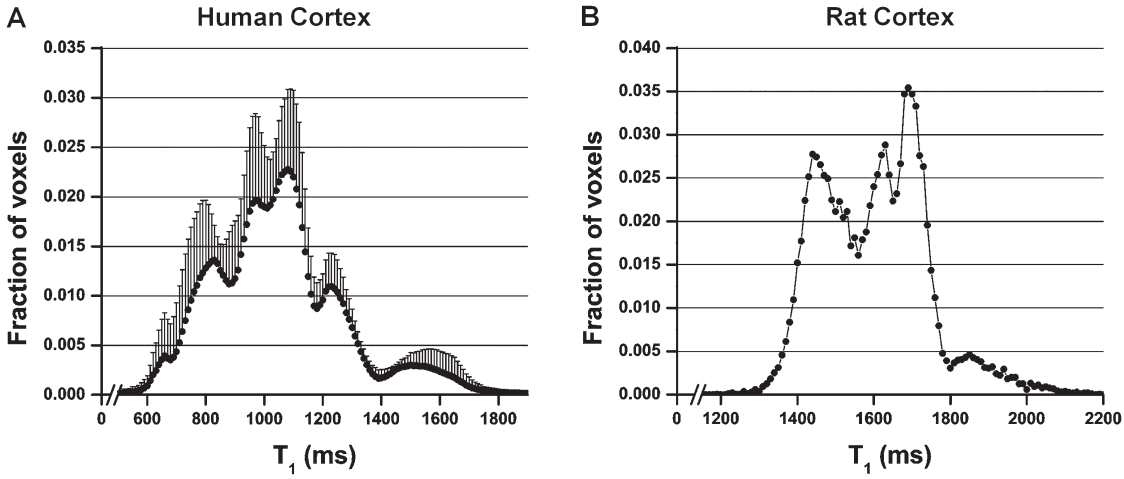

Figure 1. T_1 distribution of the cortex. (*A*) A histogram of the longitudinal relaxation time (T_1) distribution across the entire cortex averaged for 6 subjects (that were measured with slice thickness of 1.5 mm) scanned at 3-T MRI scanner. Gaussian mixture analysis revealed that the histogram can be characterized with 6 distinct Gaussians centered at 660, 820, 970, 1080, 1220, and 1540 ms. Error bars represent standard deviations across subjects. (*B*) T_1 histogram across the rat cortex scanned at 7-T MRI scanner. Similar multi-Gaussian pattern was revealed with 5 distinguishable peaks. Note that the cortical T_1 characteristics were shifted toward ~1500 ms due to the magnitude of the magnetic field (7T > 3T).

series of ethanol (100%, 96%, and 70%), and sections were washed twice with distilled water for 15 min.

Pretreatment for cytoarchitecture staining was performed by placing the slides in formic acid 4% for 3 h. The slides were then stained overnight in a mixed solution of formic acid, double distilled water (DDW), and hydrogen peroxide, followed by several washings with DDW. The slides were either stained for cell bodies using the modified Gallyas staining for paraffin sections (Merker 1983) or stained for myelin with the Gallyas silver technique (Gallyas 1979), modified for slide-mounted tissue, similar to Zilles (Zilles 1985). The cytoarchitecture and myelo architecture sections of the whole brain were digitized with a stereotactic microscope (V12 Lumar, Zeiss, Oberkochen, Germany).

Results

The main finding of this study is that multi IR-MRI can provide unique image contrasts that enable visualization and characterization of laminar compartments in human and rat cortices. The first evidence that IR-MRI is able to divide the human cortex into substructures is based on a histogram analysis of the T_1 values throughout the cortex. The cortex is characterized by a wide range of T_1 values rather than a specific one. Such histogram shows that the T_1 values are distributed into at least 6 clusters both in human and rat brains (Fig. 1). It should be indicated that this pattern was repeated in all human subjects and at different image resolutions (see supplementary material, additional results section—Supplementary Fig. *S*1), ruling out the possibility that the distribution stems from voxel partial volume effects (PVE). We exploited the results presented in Figure 1 and Supplementary Figure *S*1, to acquire a series of IR images at different TI that yield contrasts with high sensitivity to each of the T_1 components.

Figure 2 demonstrates the IR data set and analysis pipeline on rat cortex. Figure 2*A* shows IR-MRI images of a representative slice at different TIs depicting the large contrast shift in the cortex at different TIs. Note that at each TI, different parts of the tissue are being nulled (e.g., the CSF intensity is zeroed at TI of 2000 ms, bottom-right image at Fig. 2*A*). Figure 2*B* demonstrates the *k*-means clusters (k = 8) of a subset of the rat cortex. The 8 clusters represent 6 cortical laminar compartments, the white matter, and the CSF. The clusters found within the hippocampus and the subcortex were combined into a separate cluster (no. 9) for visualization purposes. To understand the basis for the cluster arrangement, we plotted the IR signal intensities (as shown in Fig. 2*A* but only for a subset of the cortex) on a mesh-grid colored according to their cluster assignment. Using such presentation, the T_1 characteristics of each cluster are better visualized. For example, layer no. 5 (pale green) is distinguishable from adjacent layers (6—light orange and 4—light blue) mainly by the contrast in TIs 1080 and 860 ms. Figure 2*D* shows the cluster analysis for the entire cortex of the right hemisphere. On top of the clusters, we marked 4 cytoarchitectonically defined regions: PtA (parietal association cortex), S1BF (primary sensory cortex, barrel field area), AuD (secondary auditory cortex, dorsal area), and Au1 (primary auditory cortex). Variations between these regions were demonstrated by the corticograms plots (Fig. 2*E*) based on the IR signal along the cortical axis, which allow their differentiation. These corticograms indicate that the IR profiles of different cortical regions are different and that within a region, the variation of the IR intensity along the cortical axis can be used to define the border between layers (see white arrows in AuD corticogram).

Figure 2 shows that IR-MRI enables visualization and quantification of cortical substructures; yet, their relationship to the histological cytoarchitectonic layers is not straightforward. To that end, we compared rat brain IR-MRI analysis with histological cyto- and myeloarchitectonic analysis. As shown in Figure 3 on a representative slice, changes in the lamination pattern of the MRI segmentation appeared to follow the borders between cyto- and myeloarchitectonically defined cortical regions. However, as expected, the IR layers do not have a one-to-one correspondence with the histologically defined regions, since the 2 techniques are not measuring exactly the same parameter. Nevertheless, this comparison demonstrates that there is a good relationship between the histological and IR layers and that the clustering of the MRI data into 6 layers is adequate.

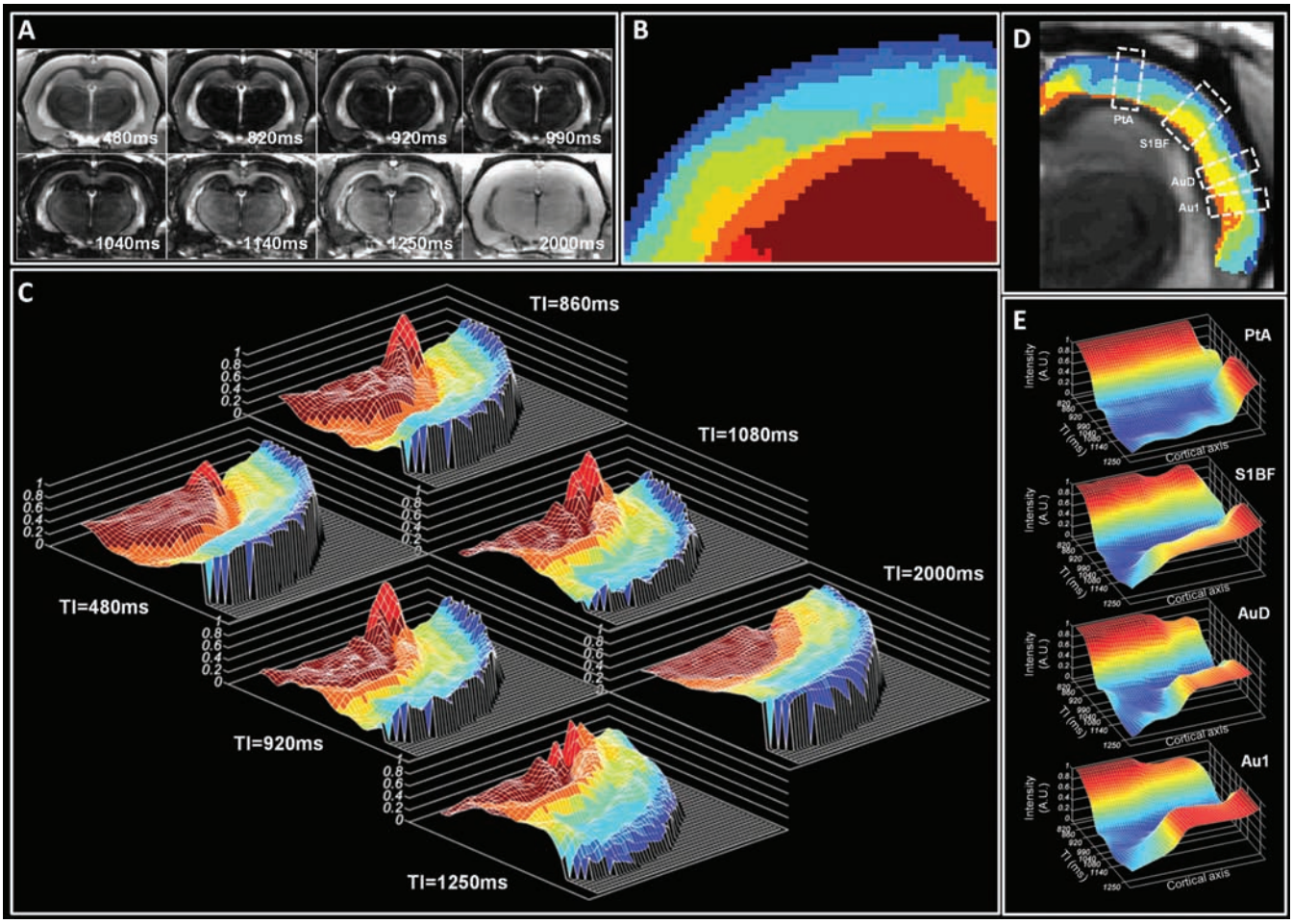

Figure 2. The cortical T_1 characteristics of the rat brain. (*A*) An IR data set of the rat brain (at TI of 480–2000 ms) was used for *k*-means clustering analysis (*B*). Eight clusters were found representing 6 cortical laminar structures, the white matter, and the CSF. The clusters found within the hippocampus and the subcortex were combined into a separate cluster (no. 9) for visualization purposes. (*C*) IR-MRI signal intensities mesh plots at different TIs of the cortical region shown in (*B*) colored according to their clustering assignment. This presentation strengthens the clustering results where each cluster is nulled at different TI. For example, CSF (marked in red) is eliminated at TI of 2000 ms, while exists at other TIs. (*D*) Cluster analysis for the entire cortex of the right hemisphere with 4 cytoarchitectonically defined regions: PtA (parietal association cortex), S1BF (primary sensory cortex, barrel field area), AuD (secondary auditory cortex, dorsal area), and Au1 (primary auditory cortex) indicated in dashed squares. Variations between these regions were demonstrated by corticograms (*E*) based on the IR-MRI signal perpendicular to the cortical axis, which allow their differentiation.

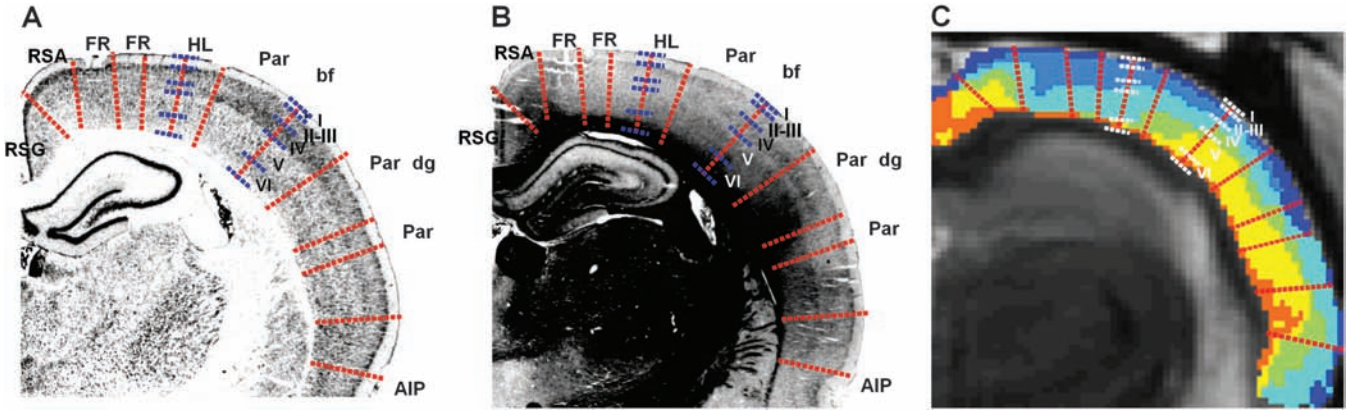

Figure 3. A comparison of IR-MRI clusters with cyto- and myeloarchitectonic analysis of the rat cortex: (*A*) cyto- and (*B*) myeloarchitectonic analysis of the rat cortex; red lines denote the cytoarchitectonic border between regions, and blue lines denote the border between the different layers. (*C*) Cluster analysis of an IR data set acquired in vivo on the rat brain; the white and yellow markings refer to the cytoarchitectonic analysis performed on histological sections of the rat brain shown in (*A*) and (*B*). Note that the IR layers resemble the histological laminar appearance, although there are some mismatches. Data indicate that the MRI laminar patterns are able to define some of the cytoarchitectonically defined borders between cortical regions.

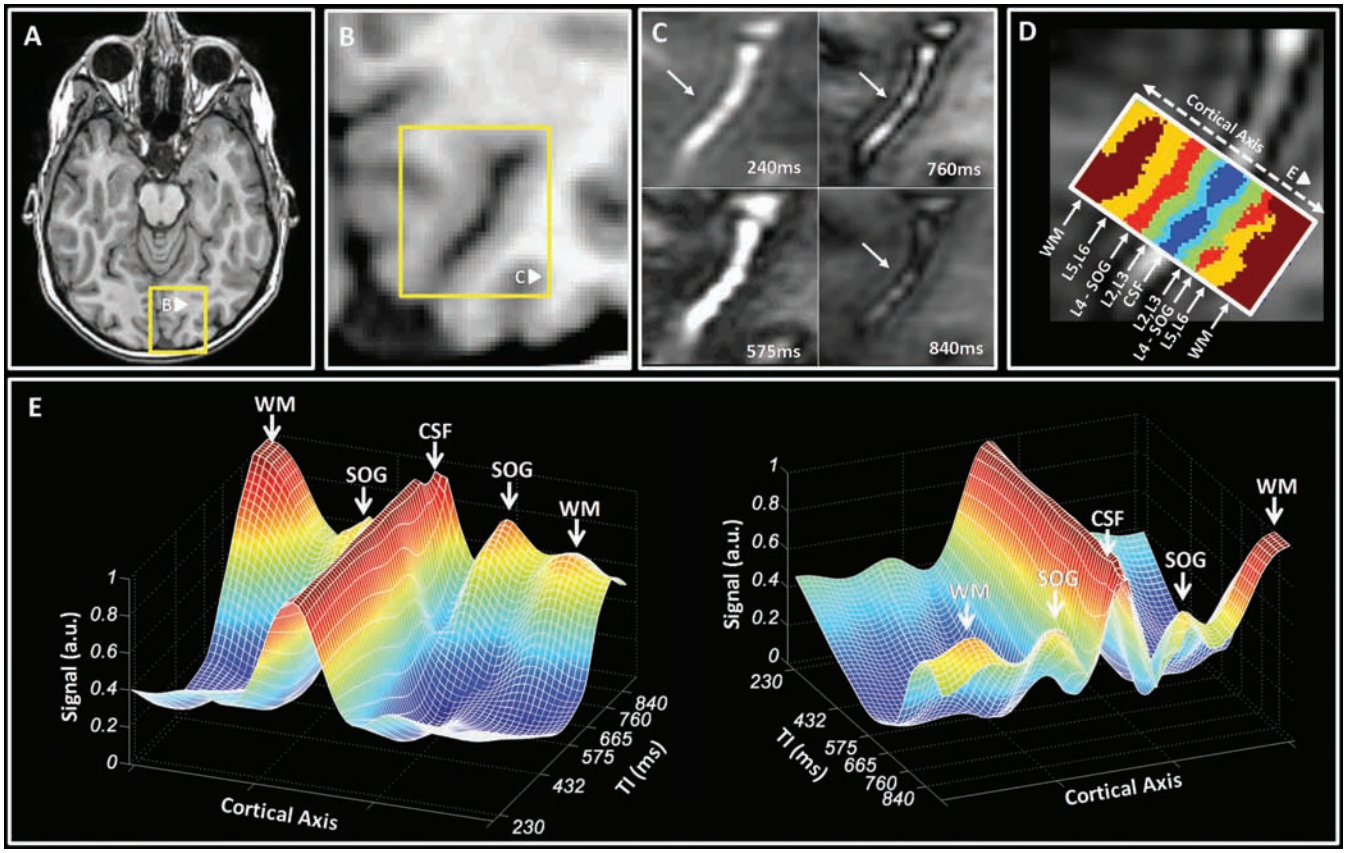

Figure 4. IR-MRI analysis resolves the cortical architecture. (*A*) An axial whole-brain SPGR with an inset containing the ROI of the primary visual cortex (i.e., BA 17) (*B*) that was further enlarged at different TIs (*C*). IR-MRI data set at different TIs provide high-contrast images of the cortex that may contribute to resolve its microstructures. For example, the heavily myelinated layer IV in BA 17 (i.e., stria of Gennari) becomes distinguishable in the TI range of 575–760 ms, known to zero most of the cortex signal. Note the bright signal band that indicates a region with similar T_1 characteristics to white matter tissue. (*D*) Clustering analysis focused on this region ascribe a specific cluster representing the stria of Gennari (red cluster). (*E*) Corticograms were computed for the clusters ROI shown in (*D*) based on the IR-MRI signal at different TIs along the cortical axis. The corticogram presentations allow detection of the stria of Gennari at several TIs according to the multipeak pattern along the cortical axis, where the stria of Gennari IR signal is similar to white matter tissue. The corticograms demonstrate the ability of IR-MRI to detect and characterize tissue's underlying architecture.

In order to demonstrate the ability of the IR contrast to resolve the cortical architecture in the human brain, we chose to focus on BA 17 (Fig. 4*A*,*B*). In that BA, the heavily myelinated layer IV (also termed stria of Gennari) should be detected with IR characteristics similar to white matter. Figure 4*C* shows IR images at different TIs at BA 17. In the TI range of 575–760 ms, known to zero most of the cortex signal, there is a bright signal band in BA 17 indicating a region with similar T_1 characteristics of white matter (Fig. 4*C* mainly in the top-right image). This region represents the stria of Gennari. These observations are reflected in a cluster analysis of the multi-IR images (Fig. 4*D*), where a specific cluster representing the stria of Gennari is obtained (red cluster). For the cluster ROI shown in Figure 4*D*, we have computed the corticograms in a similar manner to the rat data set. The corticograms (Fig. 4*E*) demonstrate the ability of IR-MRI to detect and characterize the stria of Gennari. Additional corticograms were computed to characterize other brain regions (the allocortex and motor cortex) having distinct cortical architectonic characteristics (see supplementary material, additional results section—Supplementary Figs *S*2 and *S*3). The corticogram analysis of the piriform cortex revealed only 3 IR layers while the corticogram of the motor cortex showed a prominent layer at the location of layer V.

In order to estimate the ability of IR-MRI to distinguish between cortical regions, we examined the cortical laminar compartments of the frontal lobe. These data (obtained for 6 subjects) were acquired in the sagittal plane and summarized in Figure 5. Note that at each TI a certain lamina of the cortex is zeroed (red arrows in Fig. 5*C*–*G*). As TI increases, the zone of low cortical signal (zeroed lamina) moves along the cortex until its borders are reached. According to multispectral cluster analysis, all zeroed laminae on the different IR images exhibit a laminar pattern along the cortex (Fig. 5*H*, enlarged at Fig. 5*I*), allowing quantification of the relative thickness of each of the IR layers in different regions. As Figure 5*H* clearly shows, the relative thicknesses of the different IR layers vary from region to region. For comparison, Figure 5*J*,*K* shows the normalized Brodmann's map of the same slice. Figure 5*H*,*K* shows the resemblance between the cortical regional borders defined by the Brodmann's map and the changes in laminar appearance of the IR layers.

In the following analysis, a comparison between the clusters' composition in different BAs was performed. Ten regions of the frontal lobe were selected for analysis: BAs 4, 6, 8, 9, 10, 11, 44, 45, 46, and 47. The volume fraction of each of the MRI-IR clusters was calculated for these regions and a 5 (cluster volume fraction) × 10 (BAs) repeated-measures ANOVA performed for all subjects (see Supplementary Material, additional results—Fig. *S*4). The interaction between the region and IR layer (cluster) volume fraction was highly significant

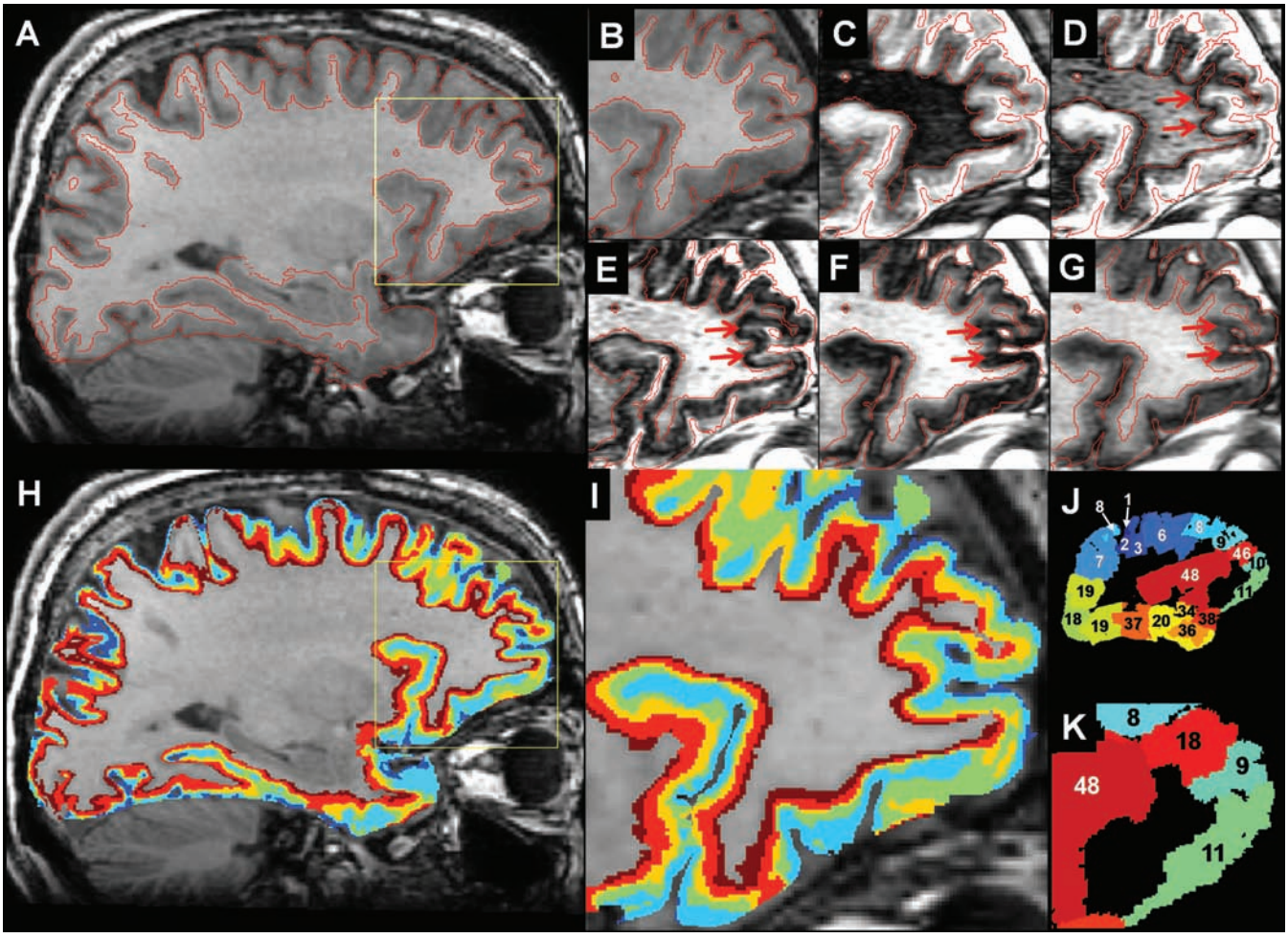

Figure 5. An IR data set of the cortex. (*A*) A sagittal SPGR T_1-weighted image of one representative slice with the cortex borders outlined in red. (*B*–*G*) Enlargement of the frontal part of cortex marked by the yellow box in (*A*) for the SPGR image (*B*): IR images with TI of 230 (*C*), 432 (*D*), 575 (*E*), 760 (*F*), and 1080 ms (*G*). The red arrows (*D*–*F*) show the propagation of the zero band of the IR along the cortex as TI increases. (*H*) A multispectral analysis of the IR images with each of the 5 clusters marked by a different color. Note that the width of each cluster varies significantly along the cortex. (*I*) An enlargement of the clustered image of frontal cortical regions in (*H*). The corresponding normalized BA maps of (*H*) and (*I*) are given in (*J*) and (*K*) for comparison. Visual inspection reveals that the changes in the laminar appearance of the cortex in the clustered maps (*H*) and (*I*) follow the Brodmann segmentation into cytoarchitectonic distinct regions (*J*) and (*K*).

($F_{36,180} = 6.6189$, $P < 0.000001$), indicating that the regions can be differentiated using the IR clusters volume fractions. Post hoc pairwise ANOVA comparison between regions revealed that 31 of the 45 possible comparisons turned out to be statistically significant (see Supplementary Table S2). The comparisons between adjacent regions are of particular interest, since if they are statistically significant, the IR layers can be used to outline the border between these regions. Eleven of the 17 comparisons between adjacent BA regions were statistically significant (9 when correcting for multiple comparisons) (Fig. 6). As the figure shows, the frontal lobe can be segmented using the IR layers into 5 regions: region 1 includes BA4, region 2 includes BAs 6 and 8, region 3 includes BAs 9, 10, and 11, region 4 includes BAs 44, 45, and 46, and region 5 includes BA 47. Thus, the IR composition of the layers differentiates between anatomical regions.

Discussion

The main result of this work is that a laminar pattern of cortical substructures can be identified and characterized with IR-MRI, in vivo for the whole brain, in 3D. The visualization and characterization of the cortical lamination pattern are based on the T_1 properties of the cortex. Using the high contrast of IR-MRI taken at different TIs, the IR clusters appeared to have a laminar structure, with the cluster that is characterized with low T_1 lying adjacent to the white matter and the cluster with the high T_1 lying adjacent to the CSF. This observation was obtained at various image resolutions and hence could not be attributed to image PVE. If PVE was the origin of this observation, it would have disappeared or decrease at higher resolution yet the phenomena sustain at a wide range of image resolution values. Moreover, the cortical laminar compartments were reproduced in all subjects and in both the human and rat brains. We demonstrated the ability of this method to define cortical substructures on several brain regions with different layer architecture: striate cortex (Fig. 4), allocortex (Supplementary Fig. *S2*), and motor cortex (Supplementary Fig. *S3*).

Although cortical architecture has been demonstrated with various MRI methodologies (Barbier et al. 2002; Fatterpekar et al. 2002; De Vita et al. 2003; Walters et al. 2003; Bridge et al. 2005; Clare and Bridge 2005; Eickhoff et al. 2005; Bridge and

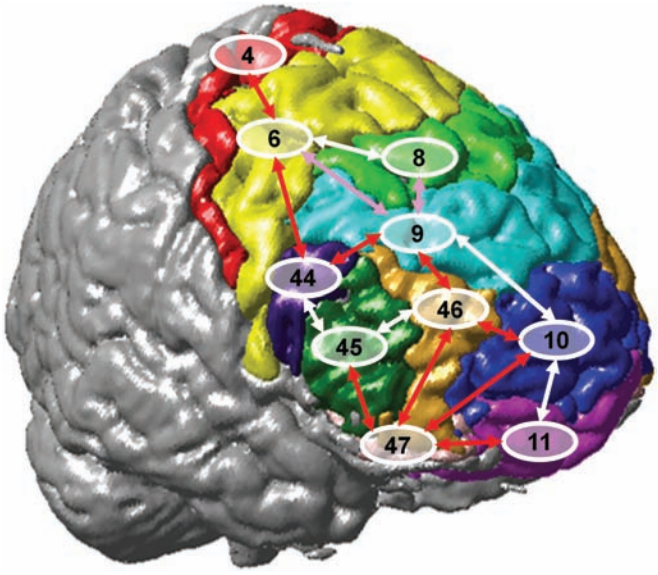

Figure 6. Statistical and regional analysis of the frontal lobe IR layer fraction. A 3D representation of one subject's anatomical T_1-SPGR scan with the normalized BAs of the frontal lobe highlighted in different colors and labeled with the BA number. The arrows are the results of a post hoc pairwise ANOVA test performed between 2 adjacent BAs' IR layer volume fractions. A white arrow denotes a nonsignificant difference (at $P < 0.05$), a red arrow denotes a significant difference that passes a Bonferroni corrected P value (depending on the number of adjacent comparisons), and a pink arrow denotes a significant difference when correction for multiple comparison is not accounted for (i.e., $P < 0.05$). Numerical values for the comparisons are given in Table S2 (see Supplementary Material).

Clare 2006; Angenstein et al. 2007; Duyn et al. 2007; Silva et al. 2008), the method presented here has several advantages: 1) it is based on standard MRI protocol and scanner setup; 2) it allows visualization of the cortical lamination patterns of the whole brain, in 3D; 3) it requires simple image processing procedures; 4) compared with other methods that demonstrate cortical laminar architecture with MRI (T_2, T_2^*, T_1, and contrast-enhanced MRI), IR-MRI yields much higher contrast, enabling a more robust identification of the layers; and 5) as consequence of the last point, high contrast for different parts of the cortex obtained by different TIs produces a multispectral data set. This is a computational powerhouse compared with a single contrast image, enabling clustering of the data based on the regional contrast profiles. Although the same data will be embedded in a T_1 calculated map, the multispectral analysis is model-free and therefore not biased by a predefined model. One limit of the multispectral approach is the need to predetermine the number of clusters. We chose 6 clusters dictated by Figure 1*A* choice that appeared to have been adequate and reasonable as these clusters have a laminar pattern and are statistically different from one another ($P < 0.0001$).

One can argue about the biological meaning of the IR layers and their histological cytoarchitecture correspondence. Although similarities were found between the cyto/meyloarchitectonic analysis and MRI parcellation, it is not claimed that the IR layers are a measure of cortical cytoarchitecture lamination pattern. It can be stated, however, that IR-MRI allows identification of cortical laminar compartments that resemble the results of cytoarchitectural segmentation. Images acquired in the rat brain showed that there is indeed not only a strong connection between the 2 measures but also some mismatches. This is not surprising since T_1 is not a direct measure of cellular architecture but rather describes the ability of the water molecules' protons to pass their magnetization to the surrounding environment. Thus, it is reasonable to expect that this parameter will be affected by tissue architecture, cellular density, and water/fat ratio (i.e., extent of myelin).

The fact that the T_1 values become shorter as one moves from the outer parts of the cortex (layers I, II) to its inner parts (layers V, VI) suggests that the tissue become more dense and rigid (evidenced by the increase of myelinated axons) and viscous, making the relaxation time shorter. However, although there is a correlation between T_1 and amount of myelin, one should be cautious about linking the 2: T_1, even when measured at high resolution as in this work, averages the contributions of many cellular components including the neurons and their processes and the glial cells and their processes. Thus, even though the degree of myelination might contribute significantly to T_1, it is not the sole parameter, and T_1 might represent both myelo- and cytoarchitecture, as was indicated in previous studies (Barbier et al. 2002).

The widths of the different lamellas of IR-MRI change significantly between cortical regions (as defined by Brodmann) (Figs 5 and 6), indicating that the IR layers have a morphological meaning and can be potentially used for regional cortical architecture studies. The segmentation of the frontal lobe into zones (e.g., BA's 6 and 8 in Fig. 6) indicates that those can be distinguished based on their IR lamination pattern. It is expected that the distinguishability between adjacent cortical regions will be different between IR-MRI and histological segmentation. Thus, the biological meaning of cortical segmentation of IR-MRI still needs to be explored. It should be noted that by acquiring additional IR images or with higher resolution (probably at higher magnetic fields > 7T), a more robust segmentation into additional regions might become feasible.

The morphological characteristics of the cortex represent a fingerprint of brain development and affect cognitive abilities and might be useful for the study of disease. The in vivo measurement of this quantity will have a tremendous impact on neuroscience, including neurobiology, psychology, and neurology. The current knowledge on brain neuroanatomical organization is gleaned from a surprisingly small number of postmortem histological samples from subjects who underwent whole-brain cytoarchitectonic analysis. Yet only in such measurements, the cytoarchitecture could be defined. However, it is argued that these samples are hardly representative of the entire population. Without underpinning the use of histological method to study brain parcellation, in vivo measurement of cortical substructures might enable large population studies in which intersubject variability can be assessed and correlated with subject-specific cognitive abilities or behavior. As brain function and brain architecture are linked (i.e., the functional and anatomical organizations of the brain are similar), measuring variations in the anatomical organization of the brain may help explain functional and behavioral differences. For example, measuring and understanding the cytoarchitecture manifestation of learning and memory, and the development of high-order cognitive skills, language, and other mental abilities, would have a huge impact on our understanding of brain function and plasticity.

Further research is needed on the methodology presented here for it to become a tool for in vivo assessment of cortical

substructures and lamination patterns. Intersubject variability over a large population data set needs to be determined. Indeed, studying the regional variation in various neurological and psychiatric diseases and disorders such as dyslexia, autism, schizophrenia, and Alzheimer's disease might shed new light on a neuroanatomical component of these diseases and its relation to disease pathogenesis and etiology. This line of research should also examine the age dependency of the layers' formation and the development of blurring between the gray matter–white matter border frequently observed at elderly subjects. Still another basic issue is the regional developmental profile of the layers from the postnatal stage to adulthood. With the potential embedded in the IR-MRI segmentation of the cortex, the above-mentioned issues could be systematically explored over large population studies. Those studies will determine the sensitivity and specificity of the proposed methodology toward cortical architecture and its temporal dynamics.

Supplementary Material

Supplementary material can be found at: http://www.cercor.oxfordjournals.org/.

Funding

German–Israeli Foundation for Scientific Research (I-2145-1652.1/2006).

Notes

The authors thank Professor Karl Zilles and Professor Katrin Amunts for their help in the histological procedures and analysis of the rat brain (Fig. 3), and Efrat Sasson, Ofer Pasternak, Ory Levy, and Shlomi Lifshits for helpful discussions. The authors also thank the Israel Science Foundation and the Raymond and Beverly Sackler Institute for Biophysics of Tel Aviv University for purchasing the 7-T MRI scanner, and the Strauss Institute for Computational Imaging of Tel Aviv University. *Conflict of Interest* : None declared.

References

Angenstein F, Niessen HG, Goldschmidt J, Lison H, Altrock WD, Gundelfinger ED, Scheich H. 2007. Manganese-enhanced MRI reveals structural and functional changes in the cortex of Bassoon mutant mice. Cereb Cortex. 17:28–36.

Annese J, Pitiot A, Dinov ID, Toga AW. 2004. A myelo-architectonic method for the structural classification of cortical areas. Neuroimage. 21:15–26.

Barbier EL, Marrett S, Danek A, Vortmeyer A, van Gelderen P, Duyn J, Bandettini P, Grafman J, Koretsky AP. 2002. Imaging cortical anatomy by high-resolution MR at 3.0T: detection of the stripe of Gennari in visual area 17. Magn Reson Med. 48:735–738.

Boretius S, Kasper L, Tammer R, Michaelis T, Frahm J. 2009. MRI of cellular layers in mouse brain in vivo. Neuroimage. 47:1252–1260.

Bridge H, Clare S. 2006. High-resolution MRI: in vivo histology? Philos Trans R Soc Lond B Biol Sci. 361:137–146.

Bridge H, Clare S, Jenkinson M, Jezzard P, Parker AJ, Matthews PM. 2005. Independent anatomical and functional measures of the V1/V2 boundary in human visual cortex. J Vis. 5:93–102.

Brodmann K, Garey L. 1999. Brodmann's localisation in the cerebral cortex. River Edge (NJ): Imperial College Press.

Clare S, Bridge H. 2005. Methodological issues relating to in vivo cortical myelography using MRI. Hum Brain Mapp. 26:240–250.

Clark VP, Courchesne E, Grafe M. 1992. In vivo myeloarchitectonic analysis of human striate and extrastriate cortex using magnetic resonance imaging. Cereb Cortex. 2:417–424.

De Vita E, Thomas DL, Roberts S, Parkes HG, Turner R, Kinchesh P, Shmueli K, Yousry TA, Ordidge RJ. 2003. High resolution MRI of the brain at 4.7 Tesla using fast spin echo imaging. Br J Radiol. 76:631–637.

Duyn JH, van Gelderen P, Li TQ, de Zwart JA, Koretsky AP, Fukunaga M. 2007. High-field MRI of brain cortical substructure based on signal phase. Proc Natl Acad Sci U S A. 104:11796–11801.

Eickhoff S, Walters NB, Schleicher A, Kril J, Egan GF, Zilles K, Watson JD, Amunts K. 2005. High-resolution MRI reflects myeloarchitecture and cytoarchitecture of human cerebral cortex. Hum Brain Mapp. 24:206–215.

Fatterpekar GM, Naidich TP, Delman BN, Aguinaldo JG, Gultekin SH, Sherwood CC, Hof PR, Drayer BP, Fayad ZA. 2002. Cytoarchitecture of the human cerebral cortex: MR microscopy of excised specimens at 9.4 Tesla. AJNR Am J Neuroradiol. 23:1313–1321.

Gallyas F. 1979. Silver staining of myelin by means of physical development. Neurol Res. 1:203–209.

Merker B. 1983. Silver staining of cell bodies by means of physical development. J Neurosci Methods. 9:235–241.

Silva AC, Lee JH, Wu CW, Tucciarone J, Pelled G, Aoki I, Koretsky AP. 2008. Detection of cortical laminar architecture using manganese-enhanced MRI. J Neurosci Methods. 167:246–257.

Vogt O. 1911. Die myeloarchitektonik des isocortex parietalis. J Psychol Neurol. 18:379–390.

von Economo CB, Koskinas GN. 1925. The cytoarchitectonics of the adult human cortex. Berlin (Germany): Julius Springer Verlag.

Walters NB, Egan GF, Kril JJ, Kean M, Waley P, Jenkinson M, Watson JD. 2003. In vivo identification of human cortical areas using high-resolution MRI: an approach to cerebral structure-function correlation. Proc Natl Acad Sci U S A. 100:2981–2986.

Yovel Y, Assaf Y. 2007. Virtual definition of neuronal tissue by cluster analysis of multi-parametric imaging (virtual-dot-com imaging). Neuroimage. 35:58–69.

Zilles KJ. 1985. The cortex of the rat: a stereotaxic atlas. Berlin (Germany): Springer-Verlag.